International Journal of Heat and Mass Transfer 54 (2011) 3874–3881

Contents lists available at ScienceDirect

International Journal of Heat and Mass Transfer

journal homepage: www.elsevier.com/locate/ijhmt

Effective thermal conductivity of functionally graded random micro-heterogeneous materials using representative volume element and BEM

Marco Dondero *, Adrián P. Cisilino, José M. Carella, J. Pablo Tomba

Research Institute of Material Science and Technology (INTEMA-CONICET), Faculty of Engineering, National University of Mar del Plata, 7600 Mar del Plata, Argentina

ARTICLE INFO

Article history:
Available online 17 May 2011

Keywords:
Effective thermal conductivity
Random composites
Boundary Element Method
Homogenization
Representative volume element
Functionally graded materials

ABSTRACT

This work introduces a numerical methodology for the computation of the effective thermal conductivity (ETC) of random micro-heterogeneous materials using representative volume elements and the Fast Multipole Boundary Element Method (FMBEM). The methodology is applied to solve two-dimensional foam-like materials consisting of random distributions of circular isolated holes. The computed ETC values are successfully used to predict the temperature fields of two materials with functionally graded ETCs. Numerical and analytical results are experimentally validated. The proposed methodology is flexible and versatile, as it is capable to account for both, the geometrical and topological details of the material microstructure.

1. Introduction

Effective thermal conductivity (ETC) of micro-heterogeneous materials has been an active research field for over a century. The importance of micro-heterogeneous materials like granular metals and ceramics [1], fibrous composites [2], or polymeric open-cell foams [3] lies in their applications in high performance insulations [4,5], packed beds, heterogeneous catalysts [6], composite materials and powder metallurgy [7]. The size, shape, physical properties and spatial distribution of the micro-structural constituents largely determine the macroscopic, overall behavior of these multi-phase materials. From the point of view of materials design, it would be highly attractive to tailor the material microstructure in order to obtain the desired set of macroscopic properties. One remarkable example of this concept can be found in the so-called functionally graded materials (FGM), where particular spatial variations of local material properties can be used to generate materials with a set of unique properties. The local composition of the microstructure in a composite material can be varied to obtain certain change in the local material property. For example, thin layer FGM electric/thermal ceramic systems are almost a commercial reality today [4]. The FGM concept could also be used in the production of thermoplastic polymeric foams for thermal insulation. Foams can be assimilated to a micro-heterogeneous material consisting of a thermoplastic polymer matrix that contains small cells filled with gas that may constitute an important fraction of the total volume [8]. The spatial distribution of the gas cells modifies the heat conduction properties along the material.

Several models for the computation of the ETC of micro-heterogeneous materials have been proposed in the literature. A recent review on this subject is due to Wang and Pan [9] who made a comprehensive and critical review of the most important existing models. The authors classified those models in two main groups, *theoretical* and *numerical*, the former are further subdivided in two-phase and multiphase models. The two-phase models are of interest for this work. Following Wang and Pan, two-phase models are classified into *basic*, *combined* and *network models*. The *basic models* are based on physical principles which have a closed form solution (either exact or approximate). Some examples are the Parallel, Series, the two forms of the Maxwell–Eucken model and the Effective Medium Theory (EMT) [10]. These models are theoretically based and they depend only on the volume fraction and thermal conductivity of the micro-structural constituents; on the other hand they represent idealized microstructures that can only be found in very specific cases [10–13]. Series and Parallel models assume that the physical arrangement of the components is either perpendicular or parallel to the heat flux. Alternatively, the Maxwell–Eucken model assumes a two-component dilute dispersion of spherical particles, that is, the distance between the particles is large enough to avoid distorting the local temperature field of each other (non-interacting). Overall, the Maxwell–Eucken model is unable to make predictions for high concentrations of particles where the local temperature distortions affect those of the neighboring inclusions. Two forms of the Maxwell–Eucken (M–E) model arise depending on the relative values of thermal conductivity of the continuous and the dispersed phases. The M–E 1 form is

* Corresponding author.
E-mail address: mdondero@fi.mdp.edu.ar (M. Dondero).

0017-9310/$ - see front matter © 2011 Elsevier Ltd. All rights reserved.
doi:10.1016/j.ijheatmasstransfer.2011.04.041

Nomenclature

A	area (mm^2)
Bi	Biot number
C	characteristic length (m)
e	emittance
f	void fraction
h	heat transfer coefficient ($W\,m^{-2}\,C^{-1}$)
k	thermal conductivity ($W\,m^{-1}\,C^{-1}$)
K	effective thermal conductivity ($W\,m^{-1}\,C^{-1}$)
L	side length (mm)
m	number of discrete f values in the FGM models
n	number of zones in the FGM models
N	number of degrees of freedom of the FMBEM model
Q	heat flux ($W\,m^{-2}$)
r	hole radius (mm)
T	temperature (°C)
x	x-coordinate (mm)
y	y-coordinate (mm)

Greek symbols

α	K/k_0 effective thermal conductivity relative to the matrix material

Subscripts

0	matrix material
1, 2	boundary condition identifier
disp	dispersed phase
envr	environment
i	discrete value identifier
r	radiation transfer
surf	surface

adopted if the conductivity of the matrix, k_0, is greater than the conductivity of the dispersed phase, k_{disp}, and the M–E 2 form comes up if $k_0 < k_{disp}$. Conversely, the EMT model assumes a completely random distribution of the components, with neither phase being continuous or dispersed. Besides, the effect of local distortions to the temperature distribution is averaged such that the temperature over the material is uniform. In this way, the conductivity assigned is an effective value. *Combined models* consist of the weighted mean of basic models using empirical parameters [8,10,14,15]. Thus, if experimental data is available these models provide accurate results, but they are actually non-predictive. Such models require extensive experimental data to estimate parameters that may have no physical significance. Finally, the *network models* are similar to the *combined models* in the sense they combine *basic models*, but they use much more complex arrangements connecting series or parallel elements to render the microstructure of a heterogeneous material. They are only employed for certain complex materials, such as soil or filled polymers [9].

The limitations of the above-mentioned models have driven efforts toward computational approaches (*numerical methods* in Wang and Pan classification [9]) that progressively incorporate physically-meaningful higher-level description of the micro-scale. The work load is then shifted to high performance computational methods such as BEM [16], FEM [17] and Lattice Boltzmann [18]. The structural details of every phase, as shape and size distributions, can be described in detail, and only the thermal conductivity of the phases must be determined separately. Thus, heterogeneous materials with any structural topology and thermal properties can be simulated.

The computational modeling of the material microstructure together with homogenization techniques are widely used to predict the macroscopic behavior of heterogeneous materials [17,19]. Most of the homogenization approaches make an assumption on global periodicity of the microstructure details, suggesting that the whole macroscopic specimen consists of spatially repeated unit cells [19]. A somewhat more realistic approach for the homogenization of randomly distributed phases, is to use statistically representative volume elements (RVE). In order to make the computed results reliable, the RVE sample must be selected small enough to be considered as a material point with respect to the size of the domain under analysis, but large enough to be a statistically representative sample of the microstructure. Thus, a RVE usually contains a large number of heterogeneities, and therefore the computations could be expensive. However, the computational effort is small when compared to that of the direct calculation for the complete problem domain [17].

The aim of this work is to develop a numerical approach for the prediction of the thermal conductivity of functionally graded micro-heterogeneous materials. To this end, a methodology based on the numerical modeling of RVE using the Boundary Element Method (BEM) is introduced. The Boundary Element Method (BEM) is widely used to solve many engineering problems due to its simplicity in the mesh generation, restricted only to the boundaries, and accuracy as it calculates the derivative of the potential in exact form [16]. To further improve the performance of the BEM, the Fast Multipole Boundary Element Method is used in this work to reduce the computational cost in terms of both, operations and memory requirements with respect to direct BEM formulations [21].

With the purpose of testing the predictive capabilities of the proposed methodology, two foam-like functionally graded materials are analyzed. The FGM consist of circular holes distributed in a high-thermal-conductivity aluminum continuous phase and air for the holes. Numerical predictions are compared to experimental results obtained from carefully controlled experiments.

2. Theoretical models for effective thermal conductivity

We briefly review in this section the most relevant theoretical models (*combined* and *network* type) for effective thermal conductivity, which will be used later in this paper to compare and discuss the numerical results. As mentioned before, Wang and Pan [9] and Churchill [22] have done extensive reviews of theoretical and numerical models. The well-known model due to Krischer [15] (considered a *combined model*) accounts for differences in structure using an empirical weighting factor for the Series and Parallel structures. The value of the weighting parameter must be determined experimentally and cannot be assessed mechanistically from information about the physical structure. Hence, since it is difficult to make a reasonable estimate of the Krischer parameter based on intuition, the use of this model as a prediction tool is very limited. A recent work by Jagjiwanram [14] introduced a *network*-type one-parameter model to predict the ETC for highly porous two-phase systems, where particles of irregular shape have been assumed to be distributed randomly in the continuum. Predictions were compared with experimental results for aluminum–air composites. The temperature was averaged within each phase, and

thus the material structure was assimilated to an array of equivalent thermal resistors. The resistors took the form of parallel slabs inclined at a given angle θ which was the parameter to be adjusted. Wang et al. [10] claimed that models which had an intrinsically anisotropic material assumption not always fit isotropic media, and vice versa. Recently Carson [23] revisited over 10 effective conductivity models based on components' conductivities for porous food structures. He concluded that in order to be suitable for a wide range of different structures, the ETC models need an extra parameter to account for the contact between dispersed inclusions. At the same time, Carson discouraged the use of Krischer's model (considered as a "flexible" model) for isotropic materials structures, and suggested the utilization of the Maxwell–Eucken model because it assumes isotropic physical structure. Finally, Carson proposed an algorithm in the format of a flowchart to predict the ETC using five different models. The process for the selection of the appropriate models is based on previous knowledge of the material structure, such as isotropy, known or unknown empirical parameters, type of porosity, etc.

The model due to Liang and Qu [7] has been specifically developed to deal with the ETC in gas-solid composite materials at high temperature. In this model, the concept of a local equivalent thermal conductivity is defined and used to calculate the effective thermal conductivity of the bulk material without using empirical parameters. Heat transport is considered in two mechanisms, conduction in solid and gas and thermal radiation inside the cavity. A strong assumption is made on the material structure where the porous material has a periodic structure considering the cavities as cylinders or spheres. After a homogenization analysis, an analytical solution for the model is derived which predicts the ETC in terms of the radius of the cylindrical or spherical inclusions, the porosity of the material and the thermal conductivity of the phases.

3. Numerical modeling

3.1. The Fast Multipole Boundary Element Method

The Boundary Element Method (BEM) can be considered as an efficient mesh reduction method in which the spatial dimension is reduced by one. In this way, the data preparation is simplified because the mesh generation is restricted to the model boundary only. Besides, the accuracy of the method is superior to other numerical techniques [20]. The accuracy is due to the use of Green's functions as the weighting function in its formulation, what allows the calculation of the derivative of the potential in exact form. The computational cost of the standard BEM implementation can be reduced by using the Fast Multipole Boundary Element Method (FMBEM). The FMBEM reduces the computational cost of the direct BEM, from an order of $O(N^3)$ (where N is the number of degrees of freedom of the system) to a quasi-linear. This reduction is achieved by using multilevel clustering of the boundary elements into cells, multipole series expansion for the evaluation of the fundamental solutions in the far field and an efficient iterative solver. Additionally, the multipole algorithm leads to a matrix-free calculation scheme that result in a reduction in memory requirements.

The high computational effort involved in this work motivates the utilization of the FMBEM to conduct the two-dimensional steady-state heat conduction analysis. The implementation follows that proposed by Liu and Nishimura [21]. The model boundary is discretized using constant elements (see Fig. 1). The integrals involved in the assembly of the system of equations are evaluated analytically. The system of equations is solved using a preconditioned GMRES algorithm from the *slatec* public library available at *netlib* (http://www.netlib.org/). Computations were carried out using a Debian-based GNU/Linux diskless cluster consisting of eight Intel Pentium 4 CPUs with 2 GB of RAM each. A detailed description of the implementation can be found in previous works by the authors [24,25].

A systematic study of the accuracy and performance of the FBEM can be found in Ref. [25]. In that work, convergence and tune-up studies were conducted for models with the same topology to that used in this work. It was found that best results in terms of both, accuracy and performance of the FMBEM can be ensured when using 12 expansion terms and, depending on the problem size, from 60 to 300 elements per cell. The tolerance for the GMRES convergence was set 10^{-7}. For this parameter setting, the overall relative error of the FBEM was estimated 4×10^{-4}% with respect to direct BEM.

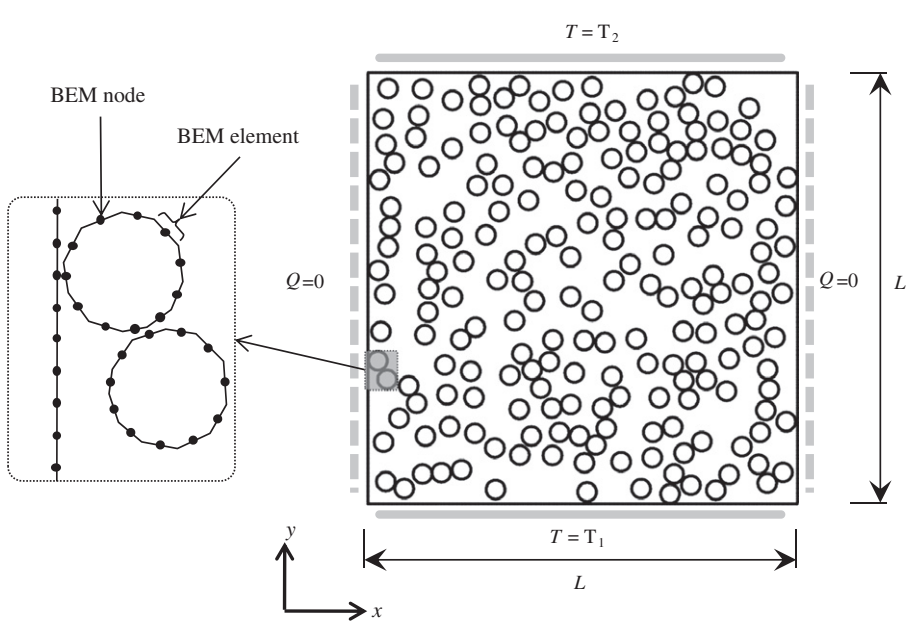

Fig. 1. FMBEM model of a representative volume element with a void area fraction $f = 0.3$ and 344 holes.

3.2. Determination of the size for the representative volume element

The material microstructure is assumed to be of the hole-matrix type in two dimensions, which may be seen as a two-dimensional idealization of, for instance, a foam microstructure with the gas cells represented by isolated holes. The matrix material is assumed isotropic. As it has been discussed in Section 1, the theoretical models are limited to work with dilute concentration of non-interacting inclusions. In this work, the interaction between particles is achieved by means of numerical modeling. Thus, the FMBEM is used to solve the Laplace equation for the isotropic steady-state heat conduction problem. The functionally graded effect is the consequence of the model topology, this is, the spatial distribution of the holes. The holes are always circular and randomly distributed. Typical microstructure geometry is illustrated in Fig. 1.

A representative volume element (RVE) is determined first in order to study the macroscopic response of the above described material. The RVE is the smallest sample of material which exhibits an invariant macroscopic response [26]. This means that the sample must be big enough to hold a representative number of heterogeneities. In order to size the RVE, a series of FMBEM analysis were performed over sets of samples with void area fractions, f, in the range $0 \leqslant f \leqslant 0.5$. Boundary conditions for the samples were specified in order to induce a global one-dimensional heat flux q in the y-direction (see Fig. 1). The normalized ETC of the micro heterogeneous material, $\alpha = K/k_0$, (where K is the ETC of the micro heterogeneous material and k_0 is the thermal conductivity of the matrix) was computed as the ratio between the heat flux through a specimen containing holes and the heat flux through a geometrically similar specimen without the holes, both for a given temperature difference between the two top and bottom sides of the specimen (see Fig. 1). The heat flux through the specimen was computed by integrating the normal derivative of temperature over the top and bottom sides of the specimens. An average of both calculated heat fluxes was used to estimate the ETC because these values are not exactly the same (as theoretically expected) due to numerical errors. Typically, heat flux values differed in less than the 0.2% between the two sides. The following number of holes per sample sequence was used to study the dependence of the effective responses on the sample size: 10, 30, 60, 100, 150, 200 and 300. The radius of the holes was set always equal to one and the size of the specimen sized in order to get the area fractions $f = 0.1$, 0.3, 0.45 and 0.5 for each holes count. In order to get statistically representative results, every computation was performed 20 times using models with a different random distribution of the holes. Each hole was discretized with 36 constant BEM elements. The same element size used in the discretization of the holes was used for the external boundary. The resulting model discretizations ranged from 504 to 13,024 elements. The solution of a model like the one illustrated in Fig. 1 on a laptop with a Pentium4 @ 3 GHz processor and 1 GB of RAM using the direct (or classical) BEM formulation took around 53 s, whereas the Fast Multipole formulation needed only 13 s. This speed difference justified the use of FMBEM for solving the $4 \times 7 \times 20 = 560$ models employed for the determination of the RVE size.

The mean and the standard deviation of the ETC results were calculated for each set of samples. The results are illustrated in Fig. 2. It can be seen that the dispersion of the data diminishes as the number of holes per sample increases. Also, an increase in the data dispersion with the void fraction is observed at low number of holes per sample. Nevertheless, this dispersion is reduced as the number of holes increases. Justified by the somewhat ad hoc fact that for two successive enlargements of the number of holes the responses differed from one another, on average, by less than 0.5%, the 200-hole samples were selected as RVE for further tests.

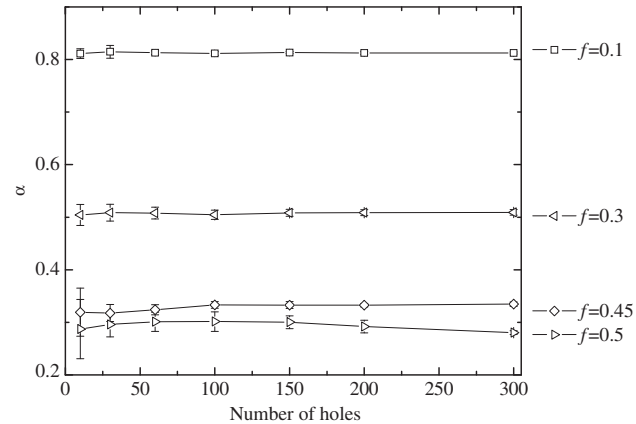

Fig. 2. Effective thermal conductivity, $\alpha = K/k_0$, as a function of the number of holes for a set of given void area fractions, f. Error bars indicate the dispersion of the results computed using 20 different random distributions of the holes.

3.3. Computation of effective properties as a function of the void-fraction

A series of 200-hole RVEs were used to compute the ETC as a function of the void fraction, $\alpha(f)$. The void area fraction range $0 \leqslant f \leqslant f_{max}$ was explored by solving the RVE models with FMBEM. The maximum void area fraction was set $f_{max} = 0.50$, as this is the maximum value attainable using the sequential addition process [27] for circular randomly-distributed holes separated by a minimum distance of $0.005r$.

Computed results are depicted in Fig. 3. The dispersion of the results (indicated using error bars which are hidden behind the symbols) is lower than 0.5% in every case. There are also plot in Fig. 3 the ETC results calculated using several analytical structural-based models: the classical Series and the Parallel models, the two forms of the Maxwell–Eucken model (see Section 1) and the Effective Medium Theory model (EMT). As expected, the homogenized FMBEM solution lays within the range limited by the Series and the Parallel (also known as the Wiener bounds). It is also observed that the computed solution lies within the range determined by the more restrictive Maxwell–Eucken models.

According to Carson et al. [28] the EMT model represents the limiting case for which the heat transfer pathway changes from through the matrix (the region over the EMT line and below the M–E 1 line in Fig. 3) to through the inclusions (the region below the EMT line and above the M–E 2 line). Hence, the region between the Maxwell–Eucken bounds may be divided into two regions with

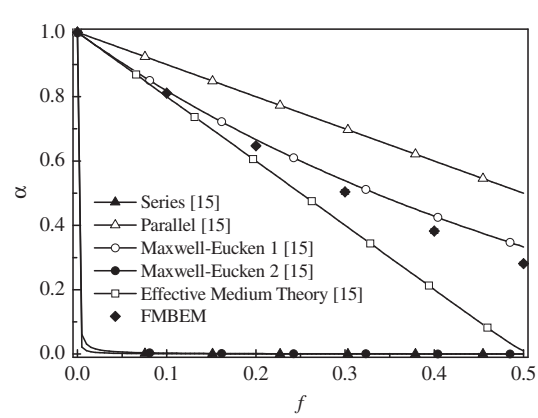

Fig. 3. Normalized effective thermal conductivity, $\alpha = K/k_0$, as a function of the void area fraction, f.

different heat transfer mechanisms. The homogenized FMBEM results lay above the EMT model and below the M–E 1 model; this is, in the zone reserved to the heat transfer mechanism through the matrix. It is worth to note that while the FMBEM solution is in good agreement with the M–E 1 model for low void area fractions (say $f < 0.10$), the difference between the two solutions augments with the increment of f. This is attributed to the interaction effects between the dispersions. The Maxwell–Eucken 1 accounts for non-interacting dispersions [10], and so, the agreement of its predictions with the computed results is good for low void area fractions where the dispersions are apart from each other. Conversely, the augment of the void fraction increases the interaction effects as the dispersions are close to each other. Under these circumstances, the predicting capability of the M–E 1 deteriorates.

The FMBEM point data can be fit with a polynomial of degree 2, from which we obtained

$$\alpha(f) = 1.0514f^2 - 1.9553f + 1 \tag{1}$$

with a correlation coefficient $R^2 = 0.9997$. This result will be used later in this work.

4. Experiment design and setup

This section is devoted to describe the experimental set up devised to validate the capability of the proposed numerical method to predict the ETC of functionally graded materials.

Two macroscopic functionally graded heat-conducting materials were constructed by machining circular holes in a highly-conductive 1100 AA-Grade aluminum plate. This design is intended to approach the theoretical case of a highly-conductive two-dimensional continuous matrix with non-conductive inclusions. The spatial distribution of the holes resulted from an optimization problem solved in a previous work [24]. The Material A (see Fig. 4a) is intended to have a two-step piece-wise ETC, while the Material B (see Fig. 5a) is intended to result in a smooth ETC variation.

For the design of the materials the domain of the plate was divided into $n = 8$ zones (bands parallel to x axis depicted in Figs. 4b and 5b) with the piecewise linear interpolation for the void area fraction, $f(y)$, in terms of $m = n + 1 = 9$ prescribed discrete values, f_i. The position of the holes were generated using the rejection method [29] with the piece-wise linear interpolation of f as distribution function. The shape of the plates was a square of size $L \times L = 150 \times 150$ mm with thickness 8 mm. The diameters of the

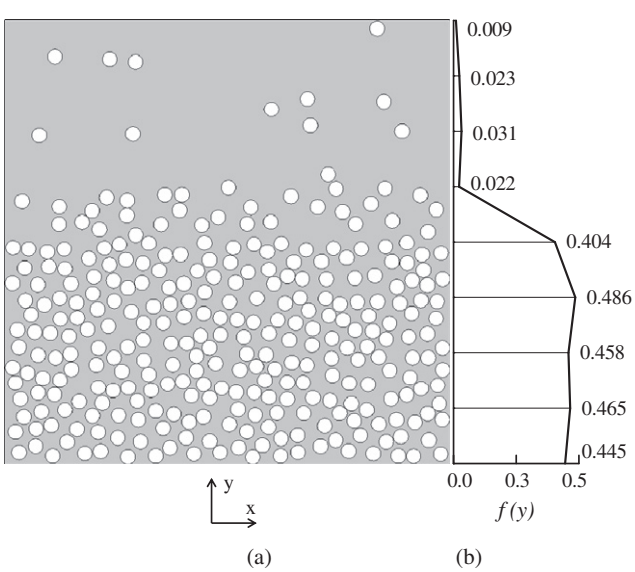

Fig. 4. (a) Distribution of the holes for the Material A, (b) void fraction distribution as a function of the position.

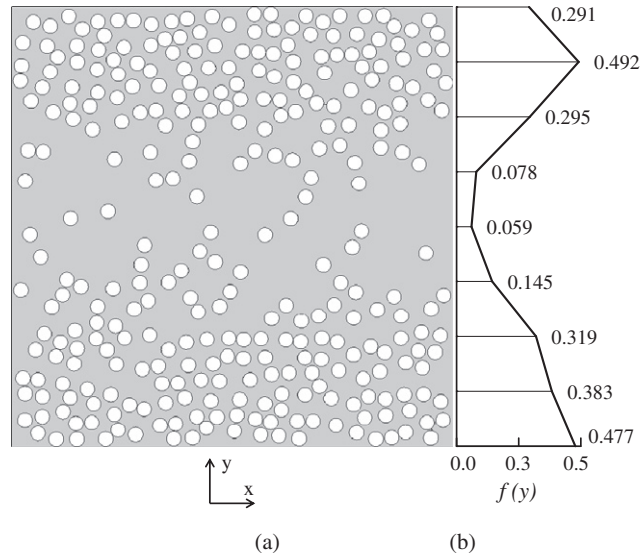

Fig. 5. (a) Distribution of the holes for the Material B, (b) void fraction distribution as a function of the position.

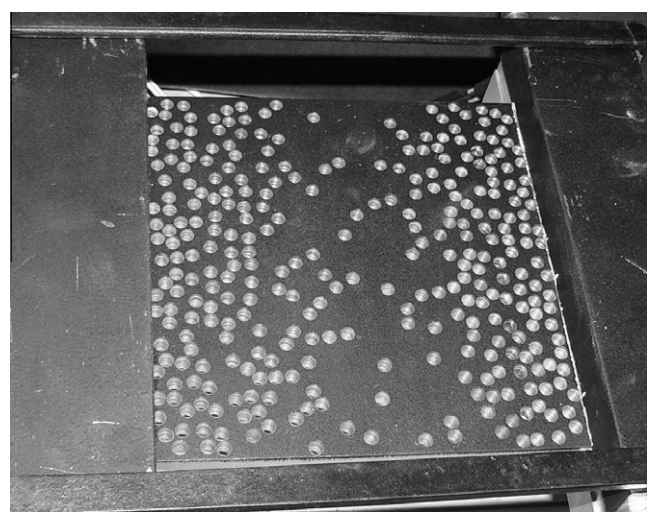

Fig. 6. Detail of the perforations in the plate.

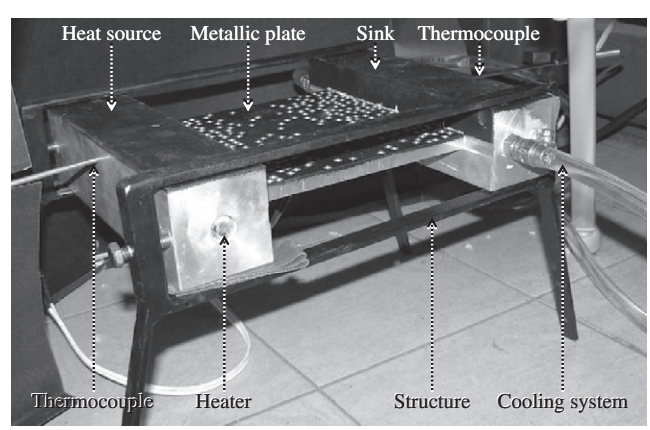

Fig. 7. Photograph of the experimental setup.

cylindrical holes were 5 mm. Holes were made using a computer controlled milling machine (see Fig. 6).

Fig. 7 illustrates the experimental setup. The actual boundary conditions used for the experiments are the same to those shown in Fig. 1. Temperatures labeled as "$T = T_2$" and "$T = T_1$" were imposed by means of a large-capacity heat source and a heat sink. The heat source was powered by a 400 W electric resistance, while the sink consisted in a water cooling system and an electric resistance used to control its temperature. The temperature of both the source and the sink were monitored using J-type thermocouples located at a minimum distance from the contact zone with the plate. The specimens were suspended horizontally on a frame to reduce natural air convection. A 1/2″ thick layer of alumina wool was placed beneath the bottom face and along the sides of the specimens in order to minimize convection and radiation heat losses. In order to obtain precise images with a thermographic camera, the top face of the plate was painted matte black to maximize and homogenize its infrared emittance. This set-up minimizes the 3d effects, making the experiment compatible with the 2d analytical and numerical models [30].

An important topic to consider is the heat transport mechanism along the specimen via the radiation across the holes. In this sense Liang and Qu [7] concluded that for a low temperature case, radiation is not important when the porosity is below 78% and the cavity diameter is less than 5 mm. Based in the previous information, the radiation inside the material is not taken into account and conductivity is considered as the only heat transport mechanism. Anyway, the holes in the specimen were plugged using alumina wool caps.

Temperature maps of the plates were measured via thermal images taken with an infrared thermographic imaging camera (Fluke Ti-30). Photographs were taken once the experiment reached the thermal steady state. The resolution of the thermal images was 120 pixels × 160 pixels, with a single temperature value assigned to each pixel. It is worth noting that the temperature values at the position of the holes did not represent true temperature data because the emittance of the alumina wool is very different to that of the matte black painted aluminum surface. Thus, the data of the thermal images were processed to delete the temperature values corresponding to the positions of holes. Different sets of temperatures T_1 and T_2 were used for each specimen. For the Material A, temperatures were $T_1 = 40$ °C and $T_2 = 200$ °C, while for the Material B, $T_1 = 35$ °C and $T_2 = 125$ °C.

5. Results and discussion

Fig. 8 shows typical data obtained with the infrared camera for the Material B. As expected, the maximum temperature gradient develops in the y-direction. In order to verify the one dimensional nature of the problem, the variation of the temperature field in the x-direction was explored. To this end, the temperature distribution along two horizontal paths at the positions $y = 64$ mm and 75 mm (slash lines in Fig. 8) are plot in Fig. 9. It can be seen that the temperature variation in the x-direction is about 3% over distances that cover about 15 times the holes diameter. Similarly, small variations in local temperature (about 6%) along the x axis can be observed over distances in the order of 2–3 holes diameters. Analogous results were obtained for analyses conducted for other positions. The previous observations allow concluding that the heat loss along the lateral faces of the specimen is negligible, and so, the data can be assimilated to those resulting for heat conduction along the y-direction only.

The temperature distributions for both materials were computed by means of FMBEM models shown in Figs. 4 and 5. Simulations were carried out using the same discretization strategy described in Section 3.1 for the analyses of the RVE. The results for the Material A and the Material B are plotted in Figs. 10 and 11 respectively as a function of the y-coordinate. Error bars for the FMBEM results indicate the dispersion of the temperatures in the x-direction. Also plotted in Figs. 10 and 11 are the experimental results, with their dispersions indicated by the gray-filled areas. The analytical solution in the figures (continuous lines) corresponds to that computed using the one-dimensional Laplace equation,

$$\frac{\partial}{\partial y}\left(k_0\alpha(f(y))\frac{\partial T}{\partial y}\right) = 0 \tag{2}$$

where $\alpha(f(y))$ is the ETC given by expression (1) specialized for the void area fraction, $f(y)$, depicted in Figs. 4b and 5b, and $k_0 = 210\ \mathrm{W\,m^{-1}\,K^{-1}}$ is the thermal conductivity of the aluminum. The boundary conditions were set the same as in the FMBEM simulation.

There is an excellent agreement between the FMBEM and the analytical solution in the whole y-coordinate range. With the only exception of the central section of the Material A (this is the position with the most abrupt variation in the temperature field) the

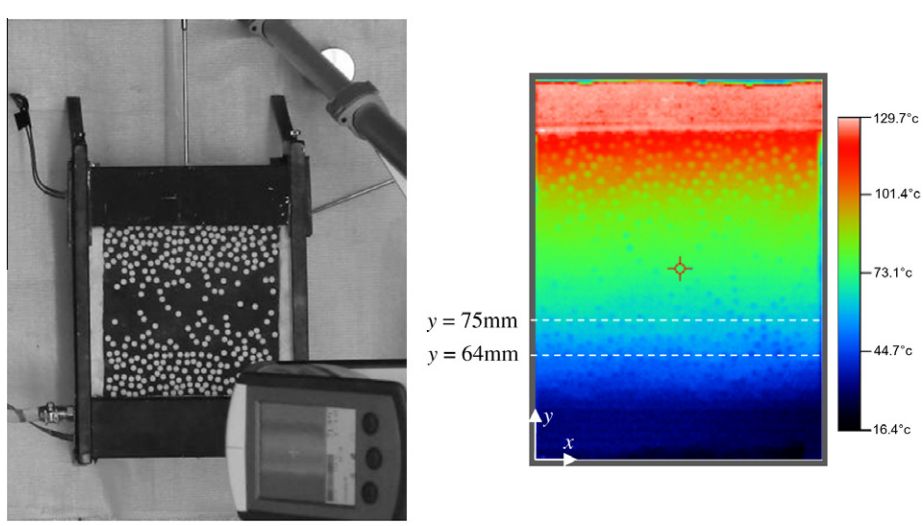

Fig. 8. Left: infrared thermographic camera taking a thermal image for the Material B. Right: thermal image showing the temperature map of the specimen, the heat source (red) and the heat sink (blue). (For interpretation of the references to color in this figure legend, the reader is referred to the web version of this article.)

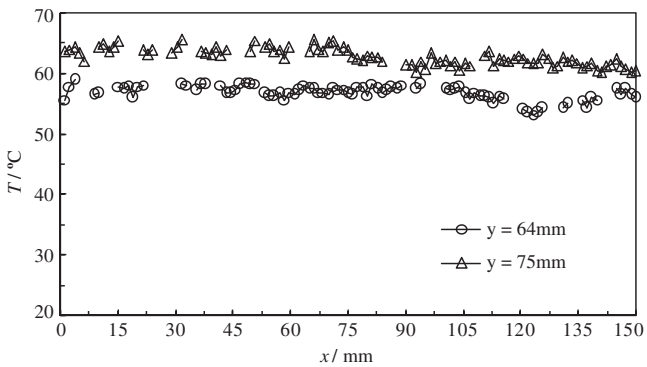

Fig. 9. Temperatures along two horizontal paths in the *x*-direction in the thermal image for Material 2.

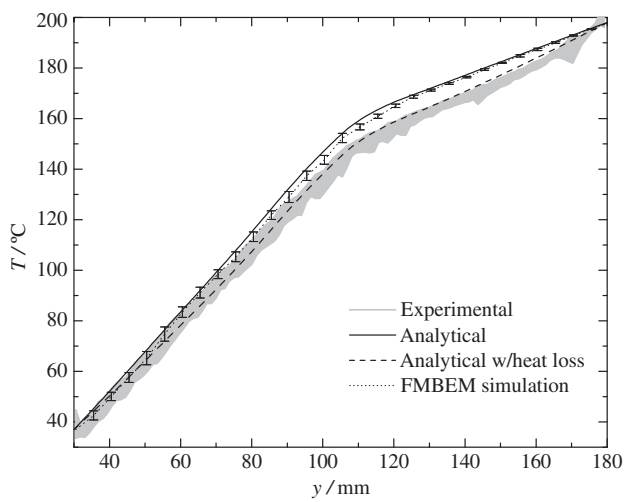

Fig. 10. Temperature distribution along the plate for the Material A.

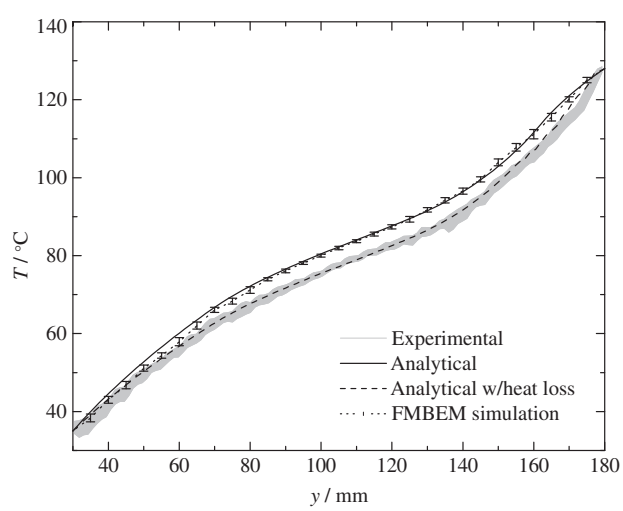

Fig. 11. Temperature distribution along the plate for the Material B.

analytical solution is within the dispersion of the FMBEM results. This accordance between the analytical and the experimental results shows the effectiveness of the expression (1) for the design of a functionally graded ETC by means of a local variation of the void area fraction.

The matching between experimental and calculated temperatures is fairly good, with deviations less than 5% for the Material A, and less than 3% for the Material B. These discrepancies between experimental, and the FMBEM and analytical results can be attributed to the heat losses on the top surface plate due radiation and convection. To ponder these effects, Eq. (2) was extended in order to include additional terms which account for the convection and radiation heat losses. This is

$$k_0\alpha(f(y))A_0\frac{dT}{dy} - hA(y)(T_{\text{surf}} - T_{\text{envr}}) - h_rA(y)(T_{\text{surf}} - T_{\text{envr}}) = 0 \quad (3)$$

where h is the convection heat transfer coefficient and $A(y)$ is the effective surface area for the heat convection and radiation. The convection coefficient was considered constant along the specimen and set $h = 4.35\ \text{W K}^{-1}\ \text{m}^{-2}$ following the estimation formula for the design of cooling air fins $h = 0.38(\Delta T)^{0.25}$, where $[h]$ = BTU ft^{-2}°F^{-1} h^{-1}, and $[\Delta T] = F$ [31]. The radiation transfer coefficient was calculated using $h_r = e\sigma(T_{\text{surf}} + T_{\text{evnr}})(T_{\text{surf}}^2 + T_{\text{envr}}^2)$ where e is the emittance, σ is the Stefan–Boltzmann constant, T_{surf} stands for the temperature on the specimen surface and T_{envr} is the environment temperature, which was set $T_{\text{evnr}} = 15$ °C. The value of the emittance was set $e = 0.95$ following Ref. [32].

Eq. (3) was solved for both materials using a one-dimensional implicit finite differences iterative scheme with the plate length discretized using 100 elements. The effective area for the heat convection and radiation, $A(y)$, was computed for each element using $A(y) = A_0(1 - f(y))$, where A_0 is the transverse area of the aluminum plate $A_0 = 150 \times 8$ mm = 1200 mm^2 and $f(y)$ the area fraction given in Figs. 4b and 5b.

The results for the analytical analysis with heat loss are plotted together with the other results in Figs. 10 and 11. It can be seen that for the Material A the results from Eq. (3) are in very good agreement with the experimental temperature values along the complete specimen; i.e. the temperature results are found to be almost inside the dispersion (grayed region) of the experimental data. For Material B, the temperature result for the analysis with heat loss lays within the dispersion of the experimental data. It is worth to remark that the analytical results with heat loss values of the convection heat transfer coefficient and the emittance in the radiation term were taken from the literature, i.e. no experimental data was fitted to determine these coefficients. This conclusion was verified using the finite difference result of Eq. (3), finding that the heat loss was 0.51% of the conduction heat transfer for Material A and 0.38% for Material B.

Finally, the Biot number [33] was estimated in order to quantify the overall heat loses due to convection and radiation. To this end, a modified version of the Biot was proposed, $Bi = C(h + h_r)/k_0$, where h and h_r account for the convection and radiation heat transfer coefficients (see Eq. (3)) respectively and C is the characteristic length, which is usually defined as the volume of the body divided by the surface area of the body. The average values for the radiation transfer coefficients, h_r, were computed using the results of the previous calculations (see Eq. (3)). These were $h_r = 9.42\ \text{W K}^{-1}\ \text{m}^{-2}$ for Material A and $h_r = 7.04\ \text{W K}^{-1}\ \text{m}^{-2}$ for Material B. The resulting values for the Biot numbers were $Bi = 2.1 \times 10^{-4}$ for Material A and $Bi = 1.7 \times 10^{-4}$ for Material B. These values of the Biot number are very low (much smaller than 1) for both materials, confirming that heat conduction along the plates predominates over the heat lose over the specimen surfaces.

6. Conclusions

It has been introduced in this work a numerical methodology for the computation of the effective (homogenized) thermal conductivity (ETC) of random micro heterogeneous materials using representative volume elements (RVE) and the Fast Multipole

Boundary Element Method (FMBEM). The methodology consists in the analysis of successive larger samples of the material microstructure in order to size the RVE, together with a statistical analysis to account for the dispersion of the results due to the random nature of the microstructure.

The methodology was applied to solve a two-dimensional foam-like microstructure consisting of a random distribution of circular isolated holes. The void area fraction of the material was considered within the range $0 \leqslant f \leqslant 0.5$. The computed ETC results were found to be in good agreement with the Maxwell–Eucken 1 model for low void area fractions (say $f < 0.10$) where the interaction effects between the holes are negligible. On the other hand, the predicting capability of the M–E 1 deteriorated (it overestimated the ETC) for high void area fractions where the interaction effects are more relevant.

The computed ETC values were used to analytically predict the temperature fields along two materials with functionally graded thermal conductivities (this is, materials with spatial variations of their void area fractions). In both cases the agreement between the analytical and numerical results (the later computed using a FMBEM model of the complete microstructure) were found very good. At the same time, the numerical and analytical results were in good agreement with the temperature fields measured with a thermographic camera in carefully controlled experiments. The effects of convection and radiation heat losses on the experiment results were estimated by means of an analytical one-dimensional model.

It can be concluded that the proposed numerical methodology is effective for the computation of the ETC of random micro heterogeneous materials. Being a numerical approach, it is capable to account for both, the geometrical and topological details of the material microstructure, thus, it can deal with inclusions of arbitrary shape. The efficient implementation using the FMBEM allows for the solution of a large number of models in a reduced time. The versatility and robustness of the methodology makes it suitable to work in combination with optimization algorithms in the design of materials with tailored conductivity properties.

Acknowledgements

This work has been partially supported by Projects PICT07-1154 and PICT06-1359 of the ANPCyT of Argentina, the National University of Mar del Plata and the CONICET of Argentina.

References

[1] M. Wang, J. Wang, N. Pan, S. Chen, Mesoscopic predictions of the effective thermal conductivity of microscale random porous media, Phys. Rev. E 75 (2007) 036702.
[2] M. Wang, Q. Kang, N. Pan, Thermal conductivity enhancement of carbon fiber composites, Appl. Therm. Eng. 29 (2009) 418–421.
[3] M. Wang, N. Pan, Modeling and prediction of the effective thermal conductivity of random open-cell porous foams, Int. J. Heat Mass Transfer 51 (2008) 1325–1331.
[4] A.J. Ruys, E.B. Popov, D. Sun, J.J. Russell, C.C.J. Murray, Functionally graded electrical/thermal ceramic systems, J. Eur. Ceram. Soc. 21 (2001) 10–11. 2025–2029.
[5] J. Kwona, C. Janga, H. Junga, T. Song, Effective thermal conductivity of various filling materials for vacuum insulation panels, Int. J. Heat Mass Transfer 52 (2009) 5525–5532.
[6] P.K. Samantray, P. Karthikeyan, K.S. Reddy, Estimating effective thermal conductivity of two-phase materials, Int. J. Heat Mass Transfer 49 (2006) 4209–4219.
[7] Liang, Qu, Effective thermal conductivity of gas–solid composite materials and the difference effect al high temperature, Int. J. Heat Mass Transfer 42 (1999) 1885–1893.
[8] S.G. Kazarian, Polymer processing with supercritical fluids, Poly Sci Ser. C 42 (2000) 78–101.
[9] M. Wang, N. Pan, Predictions of effective physical properties of complex multiphase materials, Mater. Sci. Eng. R 63 (2008) 1–30.
[10] J. Wang, J.K. Carson, M.F. North, D.J. Cleland, A new approach to modeling the effective thermal conductivity of heterogeneous materials, Int. J. Heat Mass Transfer 49 (2006) 3075–3083.
[11] E.E. Gonzo, Estimating correlations for the effective thermal conductivity of granular materials, Chem. Eng. J. 90 (2002) 299–302.
[12] E. Behrens, Thermal conductivities of composite materials, J. Compos. Mater. 2 (1968) 2–17.
[13] T.H. Bauer, A general analytical approach toward the thermal conductivity of porous media, Int. J. Heat Mass Transfer 36 (1993) 4181–4191.
[14] R.S. Jagjiwanram, Effective thermal conductivity of highly porous two-phase systems, Appl. Therm. Eng. 24 (2004) 2727–2735.
[15] O. Krischer, Die wissenschaftlichen Grundlagen der Trocknungstechnik (The Scientific Fundamentals of Drying Technology), Springer-Verlag, Berlin, 1963. Cited in English in: R.B. Keey, Drying of Loose and Particulate Materials, Hemisphere Publishing Corporation, New York, 1992 (Chapter 7).
[16] A. Sutradhar, G.H. Paulino, The simple boundary element method for transient heat conduction in functionally graded materials, Comput. Methods Appl. Mech. Eng. 193 (2004) 4511–4539.
[17] T.I. Zohdi, P. Wriggers, Introduction to Computational Micromechanics, Lecture Notes in Applied and Computational Mechanics, first ed., vol. 20, Springer-Verlag, Berlin, 2005. cc. 1, 4, 9.
[18] M. Wang, F. Meng, N. Pan, Transport properties of functionally graded materials, J. Appl. Phys. 102 (2007) 033514.
[19] V.G. Kouznetsova, Computational homogenization for the multi-scale analysis of multi-phase materials, PhD thesis, Technische Universiteit Eindhoven, Eindhoven, 2002.
[20] M.H. Aliabadi, L.C. Wrobel, The Boundary Element Method, first ed., John Wiley & Sons, Chichester, England, 2002.
[21] Y.L. Liu, N. Nishimura, The fast multipole boundary element method for potential problems: a tutorial, Eng. Anal. Boundary Elem. 30 (5) (2006) 371–381.
[22] S.W. Churchill, The thermal conductivity of dispersions and packed beds: an illustration of the unexploited potential of limiting solution correlation, in: A. Mujumdar, R. Mashelkar (Eds.), Advances in Transport Processes IV, Springer, New Delhi, 1986, pp. 394–418.
[23] J.K. Carson, S.J. Lovatt, D.J. Tanner, A.C. Cleland, Predicting the effective thermal conductivity of unfrozen porous foods, J. Food Eng. 75 (2006) 297–307.
[24] M. Dondero, A. Rodriguez Carranza, A.P. Cisilino, G. Stavroulakis, Fast multipole BEM and genetic algorithms for the design of foams with functional-graded thermal conductivity, in: Recent Advances in Boundary Element Methods, in: G.D. Manolis, D. Polyzos (Eds.), A Volume to Honor Professor Dimitri Beskos, Springer, Berlin, 2009. ISBN:978-1-4020-9709-6.
[25] M. Dondero, A.P. Cisilino, G. Stavroulakis, Implementation of a fast multipole formulation applied to the boundary element method, XVI Congreso sobre Métodos Numéricos y sus Aplicaciones ENIEF2007 – I MACI 2007, Mecánica Computacional, vol. XXVI, pp. 468–484, ISSN:1666-6070. Available from: <http://www.cimec.org.ar/ojs/index.php/mc/article/view/1221>.
[26] Z. Hashin, Analysis of composite materials – a survey, J. Appl. Mech. 50 (1983) 481–505.
[27] S. Torquato, Random Heterogeneous Materials, Microstructures and Macroscopic Properties, Springer-Verlag New York, Inc.,, New York, NY, 2002.
[28] J.K. Carson, S.J. Lovatt, D.J. Tanner, A.C. Cleland, Thermal conductivity bounds for isotropic, porous materials, Int. J. Heat Mass Transfer 48 (2005) 2150–2158.
[29] W.H. Press, S.A. Teukolsky, W.T. Vetterling, B.P. Flannery, Numerical Recipes in Fortran 77, second ed., Cambridge University Press, Cambridge, UK, 1992.
[30] M. Wang, J. Wang, N. Pan, S. Chen, J. He, Three-dimensional effect on the effective thermal conductivity of porous media, J. Phys. D: Appl. Phys. 40 (2007) 260–265.
[31] W.H. Mc Addams, Heat Transmissions, second ed., Mc Graw-Hill, New York, United States, 1942.
[32] F. Kreith, J.F. Kreider, Principles of Solar Engineering, first ed., Mc Graw-Hill, Washington, United States, 1978.
[33] F.P. Incropera, D.P. DeWitt, T.L. Bergman, A.S. Lavine, Fundamentals of Heat and Mass Transfer, sixth ed., John Wiley and Sons, Hoboken NJ, US, 2007. ISBN:10-0471457280.